

ON THE NUCLEAR FRAGMENTATION MECHANISMS IN NUCLEAR COLLISIONS AT INTERMEDIATE AND HIGH ENERGIES

AL. JIPA¹, C. BEŞLIU¹, D. FELEA², B. ILIESCU¹, O. RISTEA¹, C. RISTEA², M. CĂLIN¹, A.
HORBUNIEV¹, I. ARSENE², T. EŞANU¹, S. OCHEŞANU¹, C. CARAMARCU¹, C.
BORDEIANU¹, I. ROŞU¹, I.V. GROSSU¹, I.S. ZGURĂ², E. STAN², C. MITU², M. POTLOG², M.
CHERCIU¹, I. ŞTEFAN²

¹ *Faculty of Physics, University of Bucharest, Bucharest-Măgurele, ROMANIA*

² *Institute of Space Sciences, Bucharest-Măgurele, ROMANIA*

(Received July 22, 2004)

Abstract. The nuclear fragmentation mechanisms can be discussed by taking into account different scales related to the fragment sizes. Considering two fragmentation mechanisms of the nuclei at the same incident energy an analysis of the experimental results obtained was done. Goldhaber formula was improved by analyzing the discrepancies between data and theories concerning the projectile fragmentation. We implied that the projectile fragmentation process would be governed by the distribution of nucleon momenta in the projectile after the collision occurred. We used in our analysis protons from the ${}^4\text{He}+{}^7\text{Li}$ at 4.5 GeV/c per nucleon incident momentum, as well as from ${}^{40}\text{Ar}+{}^{12}\text{C}$ at 213 AMeV bombarding energy. We proved that in order to proceed in analyzing the projectile fragmentation process at intermediate and high energies one has to consider the dependence of σ_0 on the apparent temperature of projectile nucleus after the collision took place. The generalized Bertsch correction for light projectile nuclei and fragments was used and the number of spatial correlations between identical nucleons having anticorrelated momenta was found. Thus we found apparent temperature values close to the separation energies of the considered fragments per number of fragments. The temperatures associated to kinetic energy spectra of the projectile fragments were calculated following two methods. The results from Bauer's method were compared with those obtained by fitting the kinetic energy distributions of the projectile fragments in the rest frame of the projectile with a Maxwellian curve. We also accomplished the comparison of the experimental results with similar events simulated with RQMD 2.4. All the results obtained suggested two nuclear fragmentation mechanisms: a sudden fragmentation by explosive mechanisms, like shock waves and a slow fragmentation by the "fission" of the spectator regions, mainly because of the interactions with the particles or fragments emitted from the participant region at transverse angles (in CMS).

Key words: nuclear fragmentation mechanism, breakup fragments, apparent temperatures, momentum distributions, kinetic energy spectra

Fragmentation processes in nuclear interactions

1. INTRODUCTION AND BACKGROUND

About 30 years ago was started the issue of explaining the mechanism of projectile fragmentation at high energies and since then more refined experimental data and new theoretical treatments of this kind of process have been brought into attention.

First experimental results [1] inferred that the projectile breakup is a fast process governed by Gaussian type momentum distribution of the nucleons in the projectile before the collision took place [2]:

$$f(P) \approx e^{-P^2/2m_\pi^2 c^2}, \quad (1)$$

where $\sigma \cong m_\pi \cdot c = 139 \text{ MeV} / c$, and $\sigma \neq \sigma(A_{\text{fragment}})$.

It was further shown [3-5] that the dispersion of the longitudinal momentum values in the frame where projectile is in rest is a function of the mass number of the fragment K in a manner well fitted by a parabolic expression:

$$\sigma^2 = \sigma_0^2 \cdot \frac{K \cdot (A - K)}{A - 1}. \quad (2)$$

Here, K is the mass number of fragment and A is the mass number of projectile. The variance σ_0^2 appear as a constant, the experimental value found being $\sigma_{0\text{exp.}} \approx 90 \text{ MeV} / c$.

If the projectile could pass a rough thermal equilibrium state instead of sudden liberation of virtual fragments, it would be obtained a similar equation to (2) [3]:

$$\sigma^2 = m_N T \cdot \frac{K(A - K)}{A}, \quad (3)$$

where m_N is the nucleon mass and the temperature T is corresponding to an excitation energy close to mean nucleon binding energy $\approx 9 \text{ MeV}$. Still, there was a discrepancy between the experimental values and theoretical ones for σ_0^2 (for ^{40}Ar and $K = 20$: $\sigma_{0\text{theor.}} \approx 1.32 \cdot \sigma_{0\text{exp.}}$ [6].

The diminution of the dispersion was achieved by including Pauli correlation [6] (e.g. for ^{40}Ca dispersion is reduced by 37% compared to 31.5% measured reduction and in addition, by presuming that the fragment is a Fermi gas [7]. The results are qualitatively improved, showing the dependence of σ_0^2 on the mass number of the fragment, including a particular behavior at $A/2$. However, the predicted fragment momentum distributions were narrower than those observed, sometimes by a large degree. By applying a kinematical semi-classical model [8], the width of the momentum distribution of a fragment was found to be sensitive to the single-particle distribution but the quantitative difference with the experiment remains. For heavy projectiles broader experimental widths could be observed than for light and medium ones [9,10].

Taking into account that the modes of projectile fragmentation are independent of the target nucleus [11-13], the above discrepancy could be understood in the view that the projectile nucleus is not a simple spectator [14] and that the projectile breakup is not a cold process [15] as it was assumed from the very beginning [3].

The mechanism of the transfer of energy and momentum to the projectile prefragment was described in [9] ($E_{\text{inc.}} = 1200$ MeV/nucleon) and in [16] ($E_{\text{inc.}} = 600$ MeV/nucleon). Using temperature measurements performed by the ALADIN group, one can find that the density of the nuclear system and the excitation energy received by the spectators during collision could be dominated by dynamical processes as shown by the IN2P3 Collaboration [16]. Their behavior could as well be explained using thermodynamical models, based on the assumption that the system passes a state of thermal equilibrium [17].

By applying the Fermi gas formula, an apparent temperature around 5.5 MeV was obtained [16], although the main conclusion was that the system included in that analysis $Au+Au$ ($E_{\text{inc.}} = 600$ MeV/nucleon) might not be in equilibrium. Apart from the aforementioned assumption made by Goldhaber on the possibility of a thermal equilibrium state to be established [3], several methods have been developed in order to estimate the excitation energy transferred to the projectile during collision [18-22]. By using the double ratios of hydrogen, helium, and lithium isotopic yields in $^{197}\text{Au}+^{197}\text{Au}$ central collisions, breakup temperatures from 5 MeV to 12 MeV were found, corresponding to an incident energy from 50 to 200 MeV/nucleon [23]. Similar values were derived, independently of the bombarding energy, from the correlated yields of light-particle coincidences [24-26].

On the other hand, under the assumption that the thermal equilibrium of the system could be achieved, the linear dependencies between the variance of the fragment velocity spectra and the fragment mass offer apparent temperature values around 30 MeV [13].

These two kinds of temperature values could be related by applying the single particle model as shown recently by Bauer in [15].

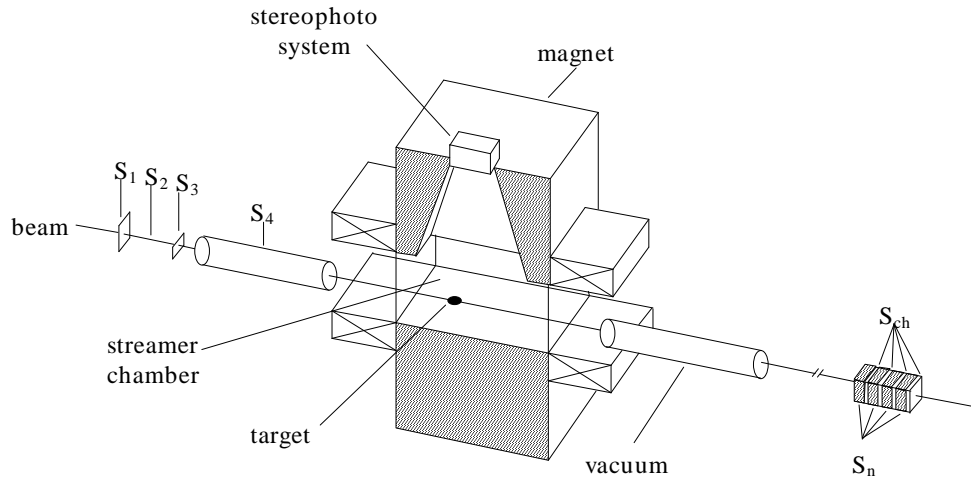
The present study shows that in order to proceed in analyzing the projectile fragmentation process at high energies, we have to take into account the dependence of σ_0^2 on the apparent temperature of projectile nucleus after the collision took place as predicted earlier [15]. The projectile fragmentation would still be a fast process, yet not as fast as it was supposed to be from the very beginning [3].

The process would be governed by the Fermi distribution of nucleon momenta in the excited projectile. Although we used a statistical method combined with Pauli exclusion principle we formulate our assumptions in the terms of an "apparent temperature" because the intrinsic mechanism of the energy transfer to the projectile is yet still unknown.

In Sec. 2 of the present paper, we present the experimental setup. Several experimental results are also discussed. Section 3 describes the formalism used. Because the fragment is a Fermi gas, the Murphy hypothesis [7] is taken into account in Subsec. 3.1. We consider the Bertsch technique [6] based on Pauli correlations for all light up to medium projectile nuclei and fragments in Subsec. 3.2. An evaluation method of the total number of possible spatial combinations between identical nucleons (in the same state of spin and isospin) having anticorrelated momenta is proposed in the same subsection. In Subsection 3.3, the projectile excitation hypothesis as suggested by Bauer [15] is applied. The connection between the obtained apparent temperatures and the nucleonic phase-space is displayed and some comments are presented in Section 4. We compare the apparent temperature of the protons as fragments of the helium nuclei, by employing two different ways in Sec. 5. Section 6 summarizes and concludes the paper.

2. EXPERIMENTAL SETUP

We used in the present analysis ${}^4\text{He}$ nuclei accelerated at the JINR Dubna Synchrophasotron,



at 4.5 GeV/c per nucleon momentum. The detection device is the SKM 200 spectrometer, shown schematically in Fig. 1 [27-29].

Fig. 1. – The SKM 200 spectrometer from JINR Dubna (Russia).

This spectrometer has a streamer chamber with the following dimensions $2\text{ m} \times 1\text{ m} \times 0.6\text{ m}$, filled with pure neon under atmospheric pressure for these experiments and placed in a magnetic field of 0.8 T. Solid targets in the form of thin disks (in the case of Li target the thickness was 1.6 g/cm^2) were mounted inside the chamber. The high voltage (500 kV/pulse, 10.5 ns length of pulse) is supplied by a Marx generator. A stereo-photographic system with three cameras allows us to record the experimental information on high sensibility films (in the case of ${}^4\text{He} + {}^7\text{Li}$ exposures two objectives were used).

The streamer chamber can be triggered with two systems of scintillation. The minimum bias triggering system for "inelastic" events, consisting of two sets of counters mounted upstream and downstream the streamer chamber, selected inelastic interactions of incident nuclei within the chamber $[T(\theta_{ch} = 0^\circ, \theta_n = 0^\circ)]$.

Here, θ_{ch} si θ_n are the minimum values of the emission angles accepted for the charged particles, fragments of the projectile nucleus with momenta higher than 3.5 GeV/c per nucleon (for these experiments), known as stripping particles, and for the neutrons respectively. The trigger efficiency was $\approx 99\%$ for one charged particle and $\approx 80\%$ for one neutron. For inelastic collisions of ${}^4\text{He}$ all charged secondaries having $p/Z > 3.5\text{ GeV}/c$ were measured regardless of the emission angle. In the present analysis, only the most statistically significant sample $T(0,0)$ was used. The

triggering system selected required projectile nuclei from a primary beam with efficiency higher than 99 %. The multiplicity distributions for inelastic interactions were corrected as described in [30].

The "central" triggering system has in the downstream part scintillation veto counters, registering a projectile and its charged fragments $\left[T(\theta_{ch} > 0^\circ, \theta_n \geq 0^\circ) \right]$. A trigger bias for central collisions is activated whenever a secondary particle from a central collision hits the veto counters and simulates a projectile-nucleus fragment. The effect was studied by simulating trajectories of secondary particles generated within the framework of the cascade model [31].

The geometry of the experimental setup and magnetic field distribution were taken into account. The corrections due to secondary interactions within a solid target turned out to be significant only for the *Li* target. The data on the multiplicity for ${}^4\text{He}+{}^7\text{Li}$ interactions were corrected for this bias [30].

Scanning, measuring and performing geometrical reconstruction obtain the experimental data. Corrections for scanning losses originate from two sources: scanning inefficiency ($\approx 2\%$) and losses of the tracks with a small projection length (which may be screened by the target container or a flash around the vertex) and/or a small curvature ($\approx 1 - 4\%$). For these experiments the absolute error in the emission angle of the stripping particles is around 10 mr for all angles, and the relative error in momentum is about 8 % for all momenta.

The SKM 200 spectrometer is detecting for charged objects only the momenta and the emission angles. The charges of the secondary particles were determined in the first phase by visual examination of the track ionization on the film. However, one cannot apply only this criterion for identifying the nuclear fragments because the estimation of the degree of ionization by ranging the streamer density is not as rigorous as for the bubble chamber. This is due to the instability of the streamer shape that leads to a large dispersion in evaluating the trace density. In exchange, a kinematical method was chosen. By observing the general distribution of the total energy, one could find for different cuts in the polar angle of the fragments [Figs. 2 (a) - 2 (d)] four Gaussian shaped peaks, centered approximately on 4.5, 6.7, 9.0, and 13.5 GeV per nucleon, corresponding to the kinematical zones associated to protons (forward and backward in the c.m.s.) [32], deuterons, and tritons (or ${}^3\text{He}$), respectively. The yields of these fragments are given in Table 1.

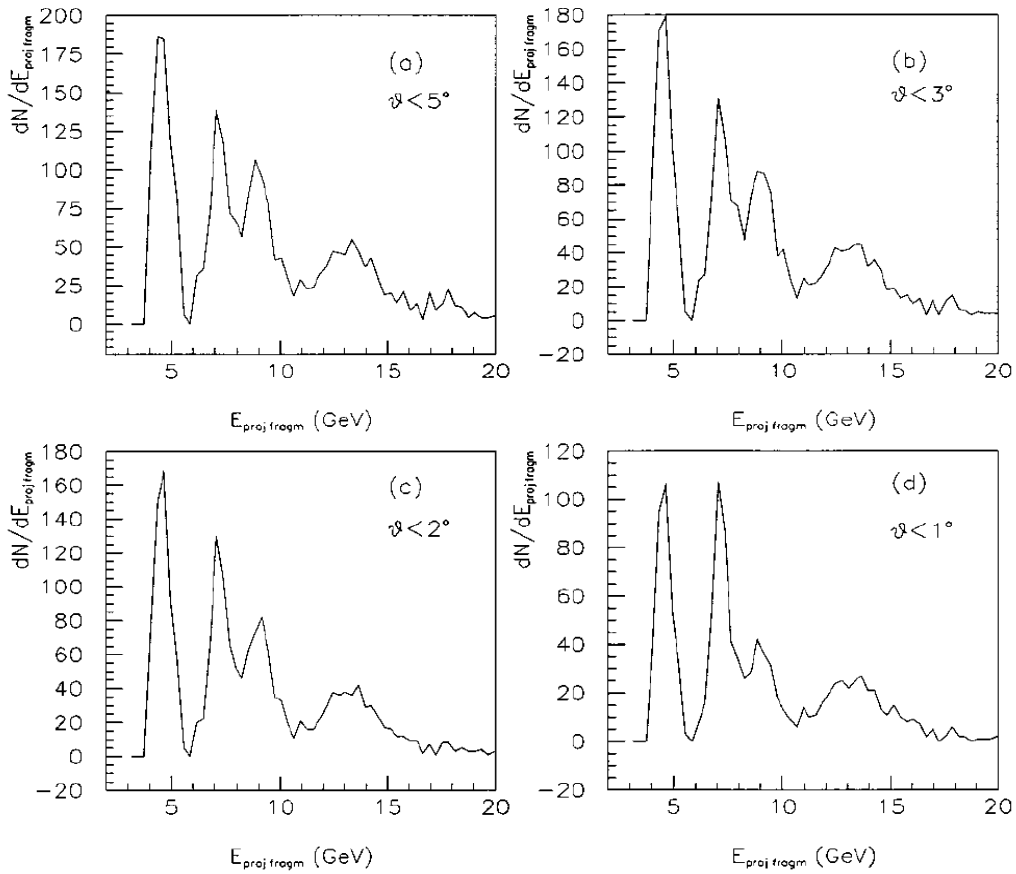


Fig. 2. – The total energy distribution in the laboratory system for positive particles with momenta higher than 3.5 GeV/c per nucleon, for ${}^4\text{He}+{}^7\text{Li}$ collisions at 4.5 GeV/c per nucleon incident momentum.

Table 1

The percentages of protons, deuterons and tritons (${}^3\text{He}$) ${}^4\text{He}+{}^7\text{Li}$ interactions at 4.5 GeV/c per nucleon incident momentum.

θ ($^\circ$)	N_{1_p} / N_{TOTAL} (%)	N_{2_d} / N_{TOTAL} (%)	N_{2_t} / N_{TOTAL} (%)
3	59.99	24.21	15.80
5	65.55	21.34	13.11
10	70.46	18.61	10.93

>10	72.00	17.66	10.34
-----	-------	-------	-------

Moreover, we have used the Relativistic Quantum Molecular Dynamics model (RQMD 2.4) for several physical hypotheses that fit best the Monte-Carlo simulated distributions with the experimental ones. Other positive particles, like π^+ and K^+ , were observed. However, the contamination percentage with these particles having momenta higher than 3.5 GeV/c to the proton momenta distributions was found to be insignificant for our study (i.e. 0.03 - 0.06 %).

We start our analysis by following a Monte-Carlo simulation technique [33,34] to determine the Fermi radius of helium projectile under the Goldhaber breakup hypothesis [3]. Despite of using the Woods-Saxon form factor for very light projectile nuclei, the obtained value $r_{F_{He}} \approx 1,6 \text{ Fm}$ looks unrealistic. One could observe (Fig. 3) an experimental Gaussian distribution of longitudinal proton momenta in the projectile rest frame for ${}^4\text{He}+{}^7\text{Li}$ interactions at $p_{inc}=4.5 \text{ AGeV}/c$. This is broader than the analogous Monte – Carlo simulated distribution having $r_{F_{He}} \approx 2,6 \text{ Fm}$ predicted by the interpolation spline function on the Moniz set of experimental data [35].

A preliminary remark might indicate, even if we do not use a transverse momentum method, that after collision an unnegligible amount of energy from nucleon-nucleon scattering was transferred to the projectile nucleus. This is reflected by a broader dispersion than for the non-excited projectile case [3]. The aforementioned remark could be strengthened by the first microscopic calculation of the spectator fragmentation [16]. By studying $Au+Au$ collisions at 600 MeV/nucleon, Gossiaux et al. found that dynamical processes dominate the excitation energy and the density of the nuclear system. By applying SACA (Simulated Annealing Cluster Algorithm) instead of MST (Minimum Spanning Tree) they found that the interaction between projectile and target increases the width of the momentum distributions considerably in comparison with that obtained from a simple Goldhaber model (for $K=5$):

$$\frac{\sigma(p_x)_{SACA} [t \geq 200 \text{ fm}/c]}{\sigma(p_x)_{Goldhaber} [t = 0 \text{ fm}/c]} \approx \frac{0,080 \text{ GeV}/c}{0,047 \text{ GeV}/c} = 1,71. \quad (4)$$

For comparison, we have obtained for protons in ${}^4\text{He}+{}^7\text{Li}$ interactions at $p_{inc}=4.5 \text{ GeV}/c$ per nucleon (Fig. 3):

$$\frac{\sigma(p_z)_{SKM200} [T \neq 0]}{\sigma(p_z)_{Monte-Carlo} [T = 0]} \approx \frac{0,1064 \text{ GeV}/c}{0,0673 \text{ GeV}/c} = 1,58. \quad (5)$$

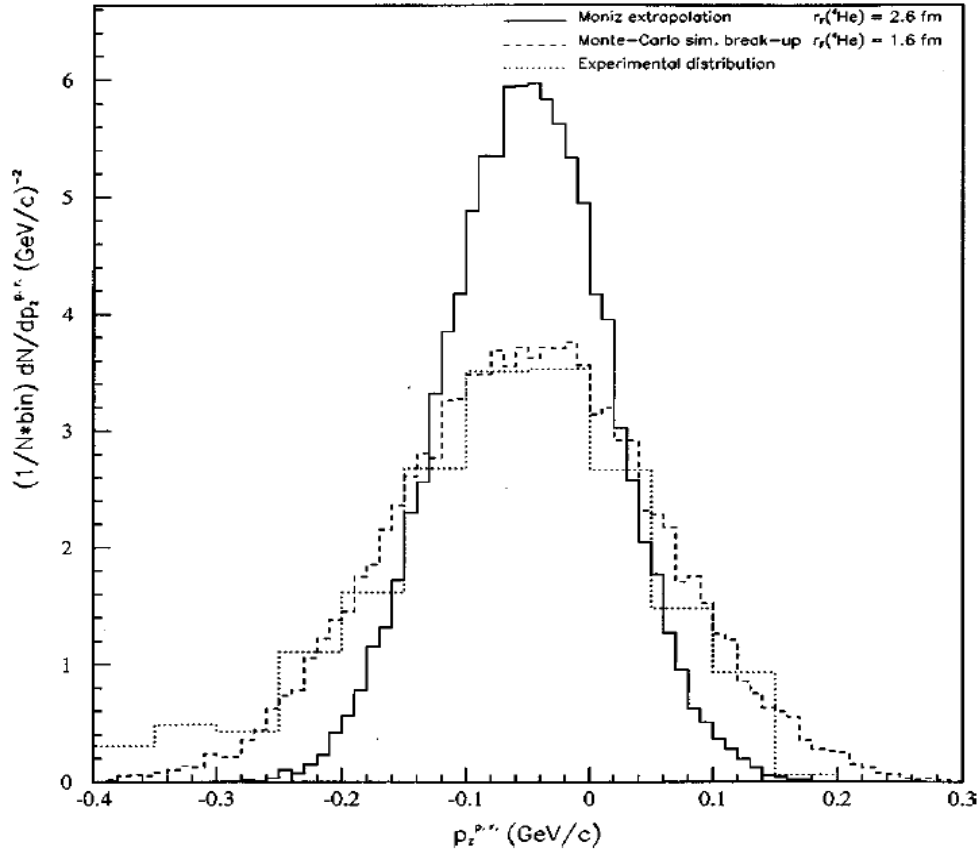


Fig. 3. – The experimental Gaussian distribution of the longitudinal proton momenta in the projectile rest frame (p.r.) for ${}^4\text{He}+{}^7\text{Li}$ interactions at $p_{\text{inc.}}=4.5$ GeV/c per nucleon compared with Monte - Carlo simulated similar distribution having $r_F(\text{He}) \sim 2.6$ fm predicted by the interpolation spline function on the Moniz set of experimental data. For comparison is given also the Monte-Carlo distribution that fits best the experimental one. The Fermi radius obtained is too small although Woods-Saxon form factor for very light projectile nuclei is applied.

A fit of Eq.(2) to the ALADIN data [13] yielding a Fermi momentum as compared with that extracted from electron scattering gives:

$$\frac{P_{F\text{ALADIN}}[\text{exp}] - P_F[T=0]}{P_F[T=0]} \approx 50\% . \quad (6)$$

Using instead for our experimental data the Fermi radius of the helium projectile nucleus as an input parameter in the simulations, and taking into account that the momentum is in inverse proportion to the nucleus radius:

$$\frac{r_{FM-C}[T=0] - r_{FSKM200}[T \neq 0]}{r_{FSKM200}[T \neq 0]} \approx 62,5 \% . \quad (7)$$

One can also notice larger widths of the distributions of the transverse components p_x and p_y in the fragmenting nucleus rest frame compared to the similar normal distributions of the longitudinal component p_z (see Fig. 4).

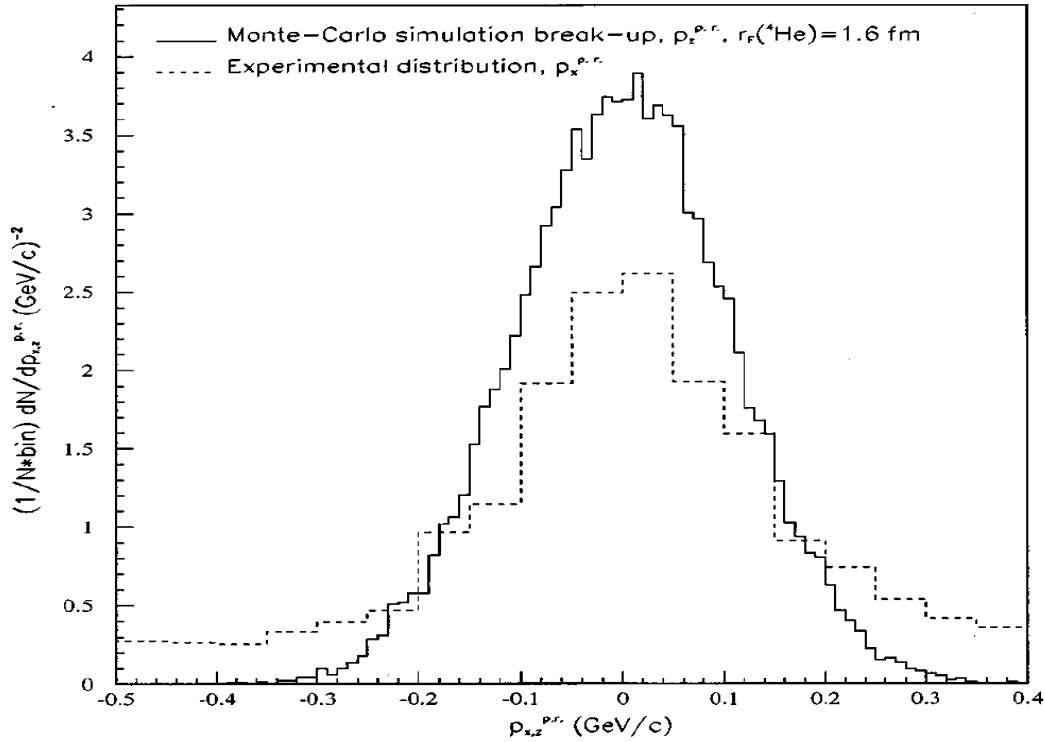


Fig. 4. – The experimental distribution of the transverse components p_x of proton momenta in the fragmenting nucleus rest frame (p.r.) and the Monte-Carlo normal distributions of the associated longitudinal components p_z for ${}^4\text{He}+{}^7\text{Li}$ collisions at $E_{\text{inc.}}=4.6$ AGeV/c.

This aspect seems to indicate that the transverse momentum analysis could be used in evaluating both the degree of thermalization for participant zone of the interaction (the so-called "fire-ball") and the degree of excitation for the projectile spectators. The topology was found to play an important role in the projectile fragmentation as shown in [12]. In order to verify this assumption one can determine the longitudinal momentum distribution widths σ_0 for different cuts in the total energy of the residual products of the projectile found within the fragmentation cone (see e.g. Figs. 5 (a) - 5 (d)).

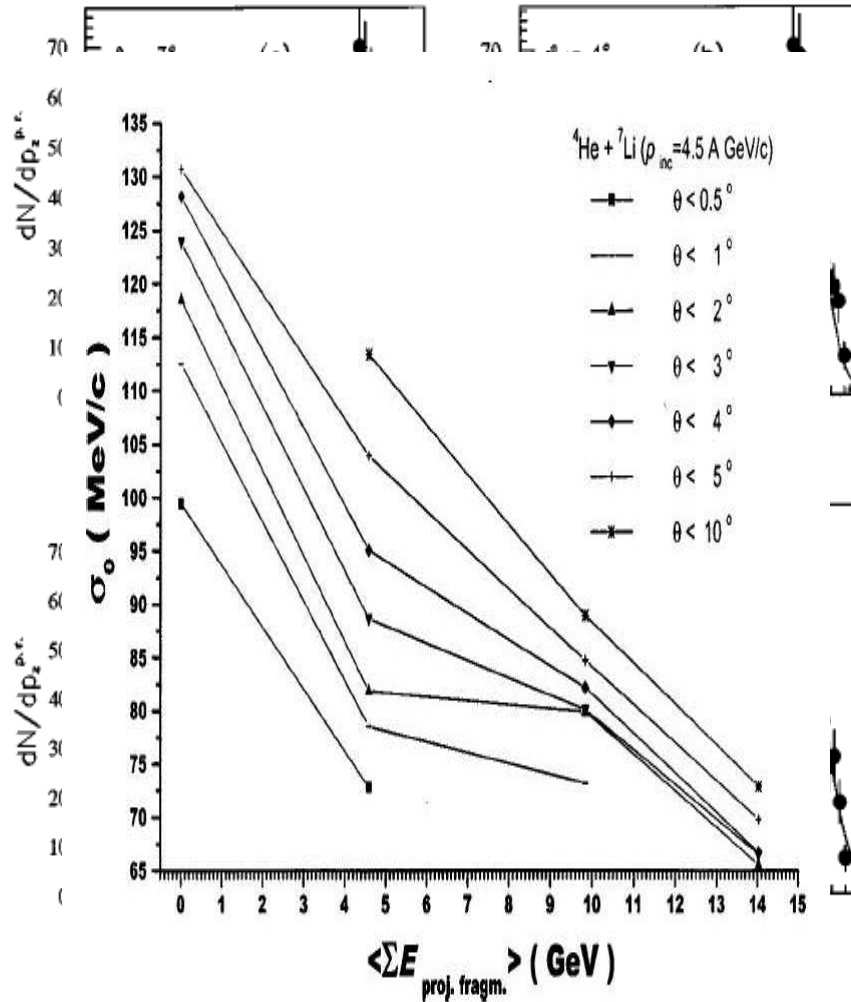


Fig. 5. – The experimental distributions of the longitudinal proton momenta in the projectile rest frame (p.r.) for ${}^4\text{He}+{}^7\text{Li}$ interactions at $p_{\text{inc}}=4.5$ A GeV/c. The solid line is a Gaussian fit for a total energy per event $3.5 \leq \sum_{\text{proj. fragm.}} E (\theta < \theta_1) \leq 5.9$ GeV and for four choices of the maximum polar angle θ_1 of the emitted projectile fragments.

These cuts could offer an estimator of the projectile-target overlap. For different forward polar angles from 0.5° to 10° we found that σ_0 is sensitive to the excitation degree of the projectile before breakup (Fig. 6).

Fig. 6. – The dependence of the distribution width of the protons momenta σ_0 measured in the helium rest frame (p.r.) with the total energy of the residual fragments of the projectile within different solid angles from 0.5° to 10° . The lines are drawn only to guide the eye.

3. FORMALISM

3.1. Murphy hypothesis

The Murphy correction factor for any fragment with K nucleons can be derived by evaluating the number of projectile states available to produce fragments $N(P_K)$ under no restriction and the same number $N'(P_K)$ considering that the fragment is also a Fermi gas (Ref. [7]):

$$\eta = \left(\frac{w'}{w} \right)_{Murphy} = \frac{N'(P_K)}{N(P_K)} = \frac{\sigma'(P_K)}{\sigma(P_K)} < 1. \quad (8)$$

We computed the dispersions of the above distributions (Figs. 7 and 8) by calculating the nucleon momentum in the projectile rest frame p_i (9), its projection on the incident axis (10) and the angle β_{ij} (11).

Therefore, we took as parameters the nucleon momentum in the fragment K 's rest frame p_j , the total momentum P_K of the fragment K in the projectile rest frame, and the angle α_j between the vectors corresponding to P_K and p_j :

$$p_i = \sqrt{\left(\frac{P_K}{K} \right)^2 + p_j^2 + 2 \cdot \left(\frac{P_K}{K} \right) \cdot p_j \cdot \cos \alpha_j}, \quad (9)$$

$$p_{z_i} = p_i \cdot \cos \beta_{ij} = \frac{P_K}{K} + p_j \cdot \cos \alpha_j, \quad (10)$$

$$\beta_{ij} = \left(\frac{\vec{P}_K, \vec{p}_i}{\hat{_K}, \hat{_i}} \right) = \arctan \left(\frac{p_j \cdot \sin \alpha_j}{\frac{P_K}{K} + p_j \cdot \cos \alpha_j} \right). \quad (11)$$

We obtained for each studied fragment the probability distributions for 50,000 events by subtracting the contribution of the Gaussian distribution.

The longitudinal momentum distribution in the projectile rest frame has an altered shape due to the restriction of the momentum conservation and a mean value far remote from zero ($\langle p_z \rangle \sim 90 \text{ MeV}/c$; Fig. 7), while the values from the distribution unaffected by Murphy hypothesis are random distributed, as expected ($\langle p_z \rangle \sim 1.5 \text{ MeV}/c$; Fig. 8).

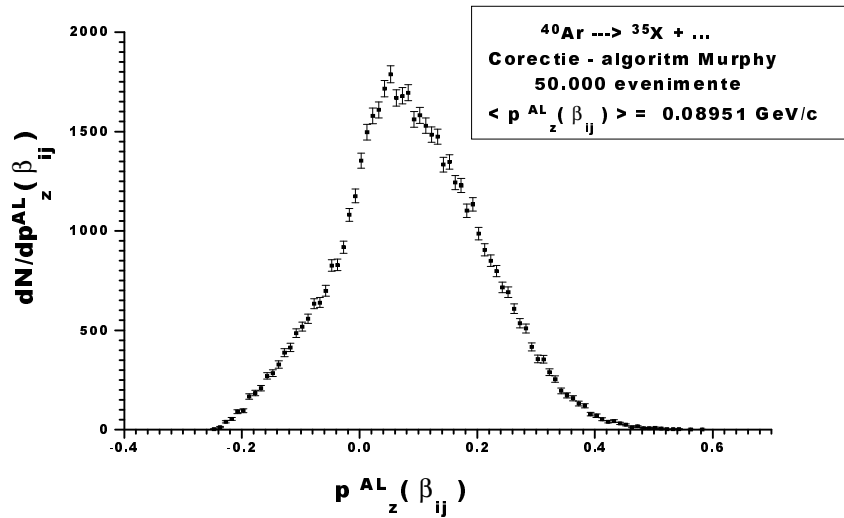


Fig. 7. – The Monte-Carlo distribution of the nucleon momenta projected on the incident axis obtained under Murphy hypothesis that the residual nucleus is also a Fermi gas.

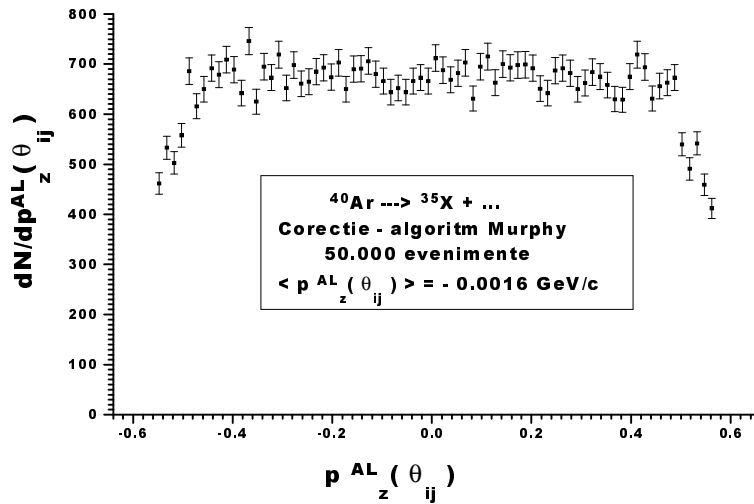


Fig. 8. – The Monte-Carlo random distribution of the longitudinal nucleon momenta obtained when no hypothesis is applied (Goldhaber theory).

3.2. The generalized Bertsch correction factor

As the Bertsch correction formula (13) concerns only the projectile nuclei and breakup fragments having completed orbits a_A and respectively a_K ($A=4a_A$; $K=4a_K$), in particular only for the ^{40}Ca incident nucleus and for $K=20$ fragment were given the results [6].

In order to obtain the generalized Bertsch correction for light up to medium nuclei where the harmonic oscillator wave function can describe the nucleons motion in the projectile nucleus, we have to evaluate the total number of spatial correlations between identical nucleons within the same state of spin and isospin and having anticorrelated momenta. Considering as Bertsch did [6] that the experiment measures the momentum on z incident direction in the disintegrating nucleus rest frame, let the operator O to have as eigenvalues the longitudinal components of nucleon momenta:

$$O = p_z \cdot f(x, y). \quad (12)$$

In a quantal description the dispersion of the longitudinal momenta for a residual fragment with a number of a orbits filled up with nucleons has the known form [6]:

$$\langle \Psi \left| \left(\sum_{i=1}^a O_i \right)^2 \right| \Psi \rangle = 4a \cdot \langle \Psi | O_i^2 | \Psi \rangle_{diag} + 4a \cdot (a-1) \cdot \langle \Psi | O_i \cdot O_j | \Psi \rangle_{id} + 12a^2 \cdot \langle O_i \cdot O_k \rangle_{non}. \quad (13)$$

The O^2 operator applies on the wave function of the projectile that could be separated in the Cartesian coordinates:

$$\Psi = F \cdot N \cdot \prod_{n=1}^a \varphi_{n_x}(x) \cdot \varphi_{n_y}(y) \cdot \varphi_{n_z}(z), \quad (14)$$

where $n=(n_x, n_y, n_z)$ represents the set of quantum numbers of the occupied orbits.

One can evaluate the matrix elements up to a normalization factor by introducing the projection operator. In order to obtain the well-known factor N_G , one has to follow Goldhaber theory [3] and consequently to avoid the Pauli correlations between nucleons in the first phase:

$$N_G = \frac{K \cdot (A - K)}{A - 1}. \quad (15)$$

For complete orbits the number of diagonal elements is $4a$, because in a quantum states we have 4 nucleons with different spin and isospin projections. The number of diagonal terms for any projectile nucleus is $N_I=K$. One can obtain the first term of the generalized Bertsch correction by using the normalization factor for the harmonic oscillator wave function:

$$\langle \Psi_k | p_z^2 | \Psi_k \rangle_{diag} = \frac{K}{A} \cdot (\pi)^{\frac{(a_K - a_A + \delta_{A,4a_A} - \delta_{K,4a_K})}{4}} \cdot \langle 0 | p_z^2 | 0 \rangle, \quad (16)$$

where $\delta_{A,4a_A}$ and $\delta_{K,4a_K}$ are Kronecker symbols corresponding to projectile respectively to the fragment having K nucleons.

The number of combinations between identical nucleons occupying the same cell from configuration space and having different projections of longitudinal momenta for ^{40}Ca nucleus type was in Bertsch theory a multiple of identical nucleon pairs in the projectile: $4A_a^2$. For a fragment with any number of nucleons K and a projectile with the mass number A , the total number of combination of this type is:

$$N_2' = 2 \cdot a_K \cdot (K - 2 \cdot a_K - 2). \quad (17)$$

Let us consider the three-dimensional momentum space splitted up into a number of $(2q)^3$ Cartesian cells. The total number of combinations between identical nucleons having randomized momenta is then $C_{(2q)^3}^2$. We have to evaluate the number of nucleon pairs with random values for transverse components (p_x, p_y) in the projectile nucleus rest frame but also with longitudinal momenta coupled: $p_z \leftrightarrow (-p_z)$, $2p_z \leftrightarrow (-2p_z)$, ..., $qp_z \leftrightarrow (-qp_z)$.

For each q value, we have $(2q)^2$ transverse cells, so the number of possible pairs for a given interval $[kp_z; (k+1)p_z]$, $\forall k = 0, (q-1)$ has to be $16q^4$. In order to obtain the physical real number of combinations between identical nucleons we have:

$$N_2 = 2 \cdot a_K \cdot (K - 2 \cdot a_K - 2) \cdot P(q), \quad (18)$$

with:

$$P(q) = \frac{16 \cdot q^5}{C_{(2q)^3}^2} = \frac{4 \cdot q^2}{8 \cdot q^3 - 1}. \quad (19)$$

Taking into account the anticorrelation between nucleon momenta, the evaluation of the second term of the dispersion gives [6]:

$$\langle \Psi | O_i \cdot O_j | \Psi \rangle_{id} = \langle \Psi | f^2 \cdot p_z \cdot (-p_z) | \Psi \rangle_{id}. \quad (20)$$

For the generalized case one can obtain:

$$\langle \Psi_k | p_i \cdot p_j | \Psi_k \rangle_{id} = -\frac{a_K^2 (K - 2 \cdot a_K - 2)^2}{a_A^2 (A - 2 \cdot a_A - 2)^2} \cdot (\pi)^{\frac{(a_K - a_A + \delta_{A,4a_A} - \delta_{K,4a_K})}{4}} \cdot \langle 0 | p_z^2 | 0 \rangle. \quad (21)$$

The factor N_3 represents the difference between the total number of possible nucleon-nucleon correlations A_{4a}^2 and the number of identical nucleons connections $4A_a^2$, i.e., $12a^2$. In general, for any light up to medium projectile and fragments:

$$N_3 = 3 \cdot a_K \cdot (a_K + 1) + (K - a_K) \cdot (K - a_K - 1). \quad (22)$$

Using the Goldhaber technique [3] in evaluating the last term of the quantum dispersion and neglecting the spatial correlations between identical nucleons, Bertsch reached the result below:

$$12a^2 \cdot \langle O_i \cdot O_k \rangle_{non} \cong \frac{3K^2}{4} \cdot \langle p_i \cdot p_k \rangle_{non} = -\frac{\langle 0 | p_z^2 | 0 \rangle}{3a} \cdot \frac{3K^2}{4}. \quad (23)$$

Following the same method as described in Refs. [3,6] and considering the mentioned correlations, it can be obtained:

$$\langle \Psi_k | p_i \cdot p_j | \Psi_k \rangle_{non} = \frac{-A + 2 \cdot a_A \cdot (A - 2 \cdot a_A - 2) \cdot P(q)}{3 \cdot a_A \cdot (a_A + 1) + (A - a_A) \cdot (A - a_A - 1)} \cdot \langle 0 | p_z^2 | 0 \rangle. \quad (24)$$

3.3. The second order approximation for dispersion

In order to introduce the dependence of Fermi momenta on the temperature, it is useful to evaluate in the second order approximation the Fermi integral:

$$I_F = \int_0^\infty G(\varepsilon) \frac{df_{FD}}{d\varepsilon} d\varepsilon = \int_0^\infty g(\varepsilon) f_{FD}(\varepsilon) d\varepsilon, \quad (25)$$

where $f_{FD} = 1/[e^{\beta(\varepsilon-\mu)} + 1]$ is Fermi-Dirac distribution function of fermions, $\beta = 1/k_B T$; the $G(\varepsilon)$ function obeys the condition $G(0) = 0$ and:

$$G(\varepsilon) = \int_0^\infty g(\varepsilon) d\varepsilon. \quad (26)$$

The Fermi integral depends on the ζ Riemann function of even arguments [36]:

$$I_F(\mu) = G(\mu) + 2 \cdot \sum_{k=1}^{\infty} G^{(2k)}(\mu) \cdot (k_B T)^{2k} \cdot \left(1 - \frac{1}{2^{2k-1}}\right) \cdot \zeta(2k), \quad (27)$$

$$\zeta(2k) = \sum_{p=1}^{\infty} \frac{1}{p^{2k}} = \frac{2^{2k-1}}{(2k)!} \cdot \pi^{2k} \cdot B_k, \quad (28)$$

where B_k represents the tabled Bernoulli numbers: ($B_1 = 1/6$; $B_2 = 1/30$).

Using a finite number of terms of the sum, an approximate form of Fermi integral results as:

$$I_F \cong G(\mu) + G^{(2)}(\mu) \cdot (k_B T)^2 \cdot \frac{\pi^2}{6} + G^{(4)}(\mu) \cdot (k_B T)^4 \cdot \frac{7\pi^4}{360}. \quad (29)$$

The last term adds an insignificant correction to the final result with respect to the experimental errors: $\leq 10^{-5}$ eV. Thus, we shall take the first two terms in order to evaluate the degree of the projectile excitation after the collision. The statistical media for the energy of fermions E_f and for the number of fermions N_f occupying a V volume and having each m_N mass, a spin $s=1/2$ and degeneracy factor $g_s=2s+1$, are, respectively:

$$E_f = \frac{g_s V}{4\pi^2} \left(\frac{2m_N}{\hbar^2} \right)^{\frac{3}{2}} \int_0^\infty \frac{\varepsilon^{\frac{3}{2}}}{e^{\beta(\varepsilon-\mu)} + 1} d\varepsilon, \quad (30)$$

$$N_f = \frac{g_s V}{4\pi^2} \left(\frac{2m_N}{\hbar^2} \right)^{\frac{3}{2}} \int_0^\infty \frac{\varepsilon^{\frac{1}{2}}}{e^{\beta(\varepsilon-\mu)} + 1} d\varepsilon \approx \frac{V}{3\pi^2} \left(\frac{2m_N \mu}{\hbar^2} \right)^{\frac{3}{2}} \left[1 + \frac{\pi^2}{8} \left(\frac{k_B T}{\mu} \right)^2 \right]. \quad (31)$$

Because the chemical potential of the fermions μ decreases very slowly with temperature, for small T values one can adopt the ratio form $k_B T / \varepsilon_F \cong k_B T / \mu$. It can be also extracted the Fermi energy from Eq.(31), taking into account that for very small temperature values the superior limit of the integral is ε_F and the Fermi-Dirac function turns into step function $f_{FD}(\varepsilon) \rightarrow \Theta_H(\mu - \varepsilon)$:

$$\varepsilon_F = \frac{\hbar^2}{2m_N} \left(3\pi^2 \frac{N}{V} \right)^{\frac{2}{3}}. \quad (32)$$

In order to evaluate the fermionic energy per nucleon and respectively the dispersion of nucleon momenta in the rest frame of the fragmenting nucleus one needs to introduce Eq.(29) in (30). In addition, to neglect the terms $\propto T^4$ and to use the Taylor first order approximation for $x \rightarrow 0$: $(1+x)^\alpha \approx 1 + \alpha x$:

$$E_f = \frac{3\mu N_f}{5} \cdot \frac{1 + \frac{5\pi^2}{8} \left(\frac{k_B T}{\varepsilon_F} \right)^2}{1 + \frac{\pi^2}{8} \left(\frac{k_B T}{\varepsilon_F} \right)^2} \approx \frac{3\varepsilon_F N_f}{5} \cdot \left[1 - \frac{\pi^2}{12} \left(\frac{k_B T}{\varepsilon_F} \right)^2 \right] \cdot \left[1 + \frac{\pi^2}{2} \left(\frac{k_B T}{\varepsilon_F} \right)^2 \right]. \quad (33)$$

$$\sigma_{0teor}^2(T) = \frac{\langle p^2 \rangle}{3} \approx \frac{p_F^2}{5} \cdot \left[1 + \frac{5\pi^2}{12} \left(\frac{k_B T}{\varepsilon_F} \right)^2 \right]. \quad (34)$$

We use from now on the natural system of units ($\hbar = c = k_B = 1$) and take into account the Bertsch generalized correction for any light and medium projectile nuclei where the approximation of harmonic oscillator wave function is considered. We also apply the Murphy correction, where the nucleons in the fragment nucleus are supposed to have Fermi distribution. Thus, the width of Fermi nucleon momenta distribution soon after the collision took place has to be [37]:

$$\sigma_{0exp} = \left(\frac{W'}{W} \right)_{Murphy} \cdot \frac{p_F}{\sqrt{5}} \cdot \sqrt{1 + \frac{5\pi^2}{12} \cdot \left(\frac{2m_N T}{p_F^2} \right)^2} \cdot \frac{\sigma_{Bertsch}}{\sigma_{Goldhaber}}, \quad (35)$$

where: $m_N = 938 \text{ MeV}$, and:

$$\left(\frac{\sigma_{\text{Goldhaber}}}{\sigma_{\text{Bertsch}}} \right)^2 = \frac{N_G \langle \Psi_k | p_z^2 | \Psi_k \rangle_{\text{diag}}}{N_1 \langle \Psi_k | p_z^2 | \Psi_k \rangle_{\text{diag}} + N_2 \langle \Psi_k | p_i \cdot p_j | \Psi_k \rangle_{\text{id}} + N_3 \langle \Psi_k | p_i \cdot p_j | \Psi_k \rangle_{\text{non}}} \quad (36)$$

One can determine the apparent temperature as function of the percentage of the nucleons having the same spin and isospin and anticorrelated projected momenta on the incident axis in the projectile rest frame:

$$T = \frac{p_F^2}{\pi \cdot m_N} \cdot \sqrt{3 \cdot \left[\left(\frac{w}{w'} \right)_{\text{Murphy}}^2 \cdot \left(\frac{\sigma_{\text{0exp}}}{p_F} \right)^2 \cdot \left(\frac{\sigma_{\text{Goldhaber}}}{\sigma_{\text{Bertsch}}} \right)^2 - \frac{1}{5} \right]} \quad (37)$$

4. DISCUSSION ON THE APPARENT TEMPERATURES

The apparent excitation temperatures T of the ^{18}Ar projectile corresponding to different breakup modes were calculated. Therefore, we used Eq.(37) based on Goldhaber formalism, with Bertsch and Murphy correction and the experimental widths obtained by Viyogi et al. [38]. Finally, we compared them with Goldhaber temperatures T_{G-V} [Eq.(3)] on the same data and with the separation energies of the considered fragments per number of fragments (Tables 2-6):

Tables 2,3

The apparent temperatures associated with breakup of ^{40}Ar into ^{16}O , ^{20}F and other fragments.

σ_{ov} [38] (MeV/ c)	q	T (MeV)	T_{G-V} [3,38] (MeV)	$E_{\text{sep./No. frag.}}$ (MeV)	Topology
78±8	1	11.69±3.94	6.65±1.36	7.47	$^{40}_{18}\text{Ar} \rightarrow ^{16}_8\text{O} + 5^4_2\alpha + 4^1_0n$
				9.56	$^{40}_{18}\text{Ar} \rightarrow ^{16}_8\text{O} + 4^4_2\alpha + 2^3_1t + 2^1_0n$
				10.70	$^{40}_{18}\text{Ar} \rightarrow ^{16}_8\text{O} + 2^4_2\alpha + ^{11}_5\text{B} + ^3_1t + 2^1_0n$
				10.71	$^{40}_{18}\text{Ar} \rightarrow ^{16}_8\text{O} + ^4_2\alpha + ^{14}_6\text{C} + ^3_2\text{He} + 3^1_0n$

	2	17.23±3.71		9.61	${}^{40}_{18}\text{Ar} \rightarrow {}^{16}_8\text{O} + {}^{22}_{10}\text{Ne} + 2_0^1n$
				13.33	${}^{40}_{18}\text{Ar} \rightarrow {}^{16}_8\text{O} + {}^{20}_9\text{F} + {}^3_1t + {}^1_0n$
89±5	1	11.71±2.61	8.66±0.97	9.68	${}^{40}_{18}\text{Ar} \rightarrow {}^{20}_9\text{F} + 4_2^4\alpha + {}^3_1t + {}^1_0n$
				10.88	${}^{40}_{18}\text{Ar} \rightarrow {}^{20}_9\text{F} + 3_2^4\alpha + {}^7_3\text{Li} + {}^1_0n$
				11.32	${}^{40}_{18}\text{Ar} \rightarrow {}^{20}_9\text{F} + 2_2^4\alpha + {}^{11}_5\text{B} + {}^1_0n$
				13.12	${}^{40}_{18}\text{Ar} \rightarrow {}^{20}_9\text{F} + 2_2^4\alpha + {}^{10}_4\text{Be} + {}^2_1d$
				11.41	${}^{40}_{18}\text{Ar} \rightarrow {}^{20}_9\text{F} + {}^4_2\alpha + {}^{15}_7\text{N} + {}^1_0n$
				13.40	${}^{40}_{18}\text{Ar} \rightarrow {}^{20}_9\text{F} + {}^4_2\alpha + {}^{14}_6\text{C} + {}^2_1d$
				17.38	${}^{40}_{18}\text{Ar} \rightarrow {}^{20}_9\text{F} + {}^{14}_6\text{C} + {}^6_3\text{Li}$
	2	18.05±2.46		17.50	${}^{40}_{18}\text{Ar} \rightarrow {}^{20}_9\text{F} + {}^{20}_9\text{F}$
				19.90	${}^{40}_{18}\text{Ar} \rightarrow {}^{20}_9\text{F} + {}^{10}_5\text{B} + {}^{10}_4\text{Be}$

Table 4

The apparent temperatures associated with breakup of ${}^{40}\text{Ar}$ into ${}^{25}\text{Mg}$ and other fragments.

σ_{ov} [38] (MeV/c)	q	T (MeV)	$T_{\text{G.v}}$ [3,38] (MeV)	$E_{\text{sep./No. frag.}}$ (MeV)	Topology
90±5	1	12.85±2.47	8.85±0.98	7.62	${}^{40}_{18}\text{Ar} \rightarrow {}^{25}_{12}\text{Mg} + 3_2^4\alpha + 3_0^1n$
				10.78	${}^{40}_{18}\text{Ar} \rightarrow {}^{25}_{12}\text{Mg} + 2_2^4\alpha + 2_1^3t + {}^1_0n$
				11.24	${}^{40}_{18}\text{Ar} \rightarrow {}^{25}_{12}\text{Mg} + {}^4_2\alpha + {}^{10}_4\text{Be} + {}^1_0n$
				12.44	${}^{40}_{18}\text{Ar} \rightarrow {}^{25}_{12}\text{Mg} + {}^4_2\alpha + {}^7_3\text{Li} + {}^3_1t + {}^1_0n$
				10.98	${}^{40}_{18}\text{Ar} \rightarrow {}^{25}_{12}\text{Mg} + {}^{14}_6\text{C} + {}^1_0n$
				13.04	${}^{40}_{18}\text{Ar} \rightarrow {}^{25}_{12}\text{Mg} + 4_1^3t + 2_1^1p + {}^1_0n$

				13.39	${}^{40}_{18}\text{Ar} \rightarrow {}^{25}_{12}\text{Mg} + {}^{11}_5\text{B} + {}^3_1\text{t} + {}^1_0\text{n}$

Table 5

The apparent temperatures associated with breakup of ${}^{40}\text{Ar}$ into ${}^{30}\text{Si}$ and other fragments.

σ_{ov} [38] (MeV/ c)	q	T (MeV)	$T_{\text{G-v}}$ [3,38] (MeV)	$E_{\text{sep./No. frag.}}$ (MeV)	Topology
92±5	2	9.09±2.71	9.25±1.01	6.32	${}^{40}_{18}\text{Ar} \rightarrow {}^{30}_{14}\text{Si} + 2_2^4\alpha + 2_0^1\text{n}$
				10.28	${}^{40}_{18}\text{Ar} \rightarrow {}^{30}_{14}\text{Si} + 2_2^4\alpha + {}^3_1\text{t} + {}^1_1\text{p} + 2_0^1\text{n}$
				10.73	${}^{40}_{18}\text{Ar} \rightarrow {}^{30}_{14}\text{Si} + 2_2^4\alpha + 2_1^3\text{t}$
	3	13.10±2.33	9.25±1.01	11.61	${}^{40}_{18}\text{Ar} \rightarrow {}^{30}_{14}\text{Si} + {}^{10}_4\text{Be}$
				12.55	${}^{40}_{18}\text{Ar} \rightarrow {}^{30}_{14}\text{Si} + 3_1^3\text{t} + {}^1_1\text{p}$

Table 6

The apparent temperatures associated with breakup of ${}^{40}\text{Ar}$ into ${}^{36}\text{S}$ and other fragments.

σ_{ov} [38] (MeV/ c)	q	T (MeV)	$T_{\text{G-v}}$ [3,38] (MeV)	$E_{\text{sep./No. frag.}}$ (MeV)	Topology
94±5	3	5.90±3.07	9.66±1.03	3.41	${}^{40}_{18}\text{Ar} \rightarrow {}^{36}_{16}\text{S} + 2_2^4\alpha$
				7.02	${}^{40}_{18}\text{Ar} \rightarrow {}^{36}_{16}\text{S} + 2_1^1\text{p} + 2_0^1\text{n}$
				8.87	${}^{40}_{18}\text{Ar} \rightarrow {}^{36}_{16}\text{S} + {}^3_1\text{t} + {}^1_1\text{p}$
	4	8.41±2.37	9.66±1.03	9.13	${}^{40}_{18}\text{Ar} \rightarrow {}^{36}_{16}\text{S} + {}^3_2\text{He} + {}^1_0\text{n}$

It can be observed that the degree of projectile fragmentation increases with the apparent excitation temperature and with the number of possible states in the momentum space. The analyzed fragmentation topology clearly shows a dependence of the received energy on the number of alpha released as confirmed in nuclear emulsion experiments [39].

Another interesting remark regards the obtained minimum q value for the fragmentation modes ${}^{40}_{18}\text{Ar} \rightarrow {}^{36}_{16}\text{S} + \dots$. For other topological modes corresponding to an equal number of one-dimensional momentum cells $2q$, the apparent temperature would be substantially greater. One deduces from the Heisenberg uncertainties relations ($\Delta z \geq \hbar/\Delta p_z$) that the dimension of the coordinate cell for the above breakup would also be higher. That indicates a smaller degree of excitation after the collision, as expected, proving that the theory is self-consistent.

By considering the interaction between projectile and target, we found that the Fermi distribution has changed. Consequently, one can notice that the width of the momentum distribution for ${}^4\text{He}+{}^7\text{Li}$ interactions as measured in the fragmenting nucleus rest frame has increased and also that the average momentum has decreased. Therefore, we believe that the Goldhaber formula [Eq.(2)] could be applied only for the fragmenting channels which implies a very small transfer of energy and momentum ($T \rightarrow 0$), or in the fragmentation of neutron-rich projectiles, where a surviving prefragment can be observed [40,41]. As for those fragmenting channels that are strongly affected by the interaction at the interface between projectile and target, the Goldhaber formula underestimates the mean square momenta of the fragments and Eq.(37) should be applied.

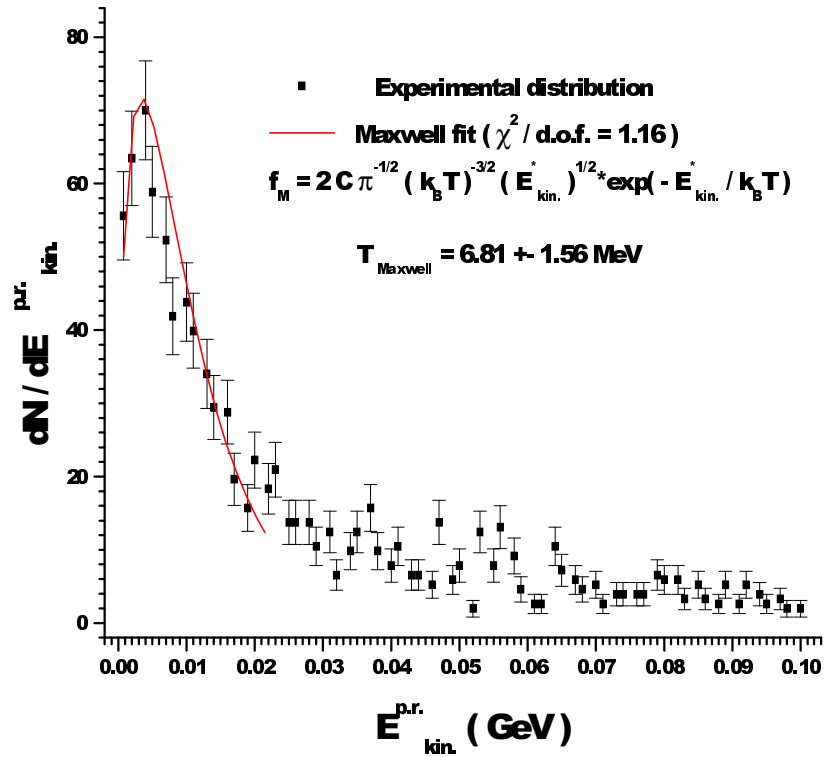
Still, a contribution of the evaporation phase to the observed mass-loss is a correction that one needs to consider further in studying heavy projectile fragmentation process where the so-called "memory effect" is no longer visible [42,43]. In this case, a higher excitation of the projectile during the formation of neutron-deficient fragments is implied by the dependence of the production yields on the neutron excess of the projectile with respect to the line of β -stability [44].

5. KINETIC TEMPERATURES OF ${}^4\text{HE}$ FRAGMENTS

We also show the results on the fragment kinetic temperatures by comparing the apparent temperature of the protons as fragments of the helium nuclei, temperature obtained in two different ways. In the first place, the temperature $T = 6.81 \pm 1.56 \text{ MeV}$ ($\chi^2 / d.o.f. = 1.16$) was obtained by fitting the kinetic energy spectra of the protons as measured in the projectile rest frame up to a normalization factor C with a Maxwellian-type distribution (Fig. 9):

$$P_{Maxwell}(E_{kin.}) = \frac{2 \cdot C}{\sqrt{\pi} \cdot T^3} \cdot \sqrt{E_{kin.}} \cdot \exp\left(-\frac{E_{kin.}}{T}\right). \quad (38)$$

Fig. 9. – The experimental kinetic energy distribution of the protons in the projectile rest frame for



$^4\text{He}+^7\text{Li}$ interactions at 4.5 A GeV/c incident momentum fitted with a Maxwellian-type curve.

The correspondent values resulted from the application of the single particle model as suggested by Bauer [15] is:

$$T = \frac{\sigma^2}{m_N}, \quad (39)$$

In order to obtain the variance of the longitudinal momentum distribution in the disintegrating nucleus rest frame one has to fit the experimental data with a Gaussian-shaped curve. Thus, we have found an apparent temperature value $T = 6.83 \pm 0.54 \text{ MeV}$ ($\chi^2 / \text{d.o.f.} = 0.996$) in good agreement with the previous one.

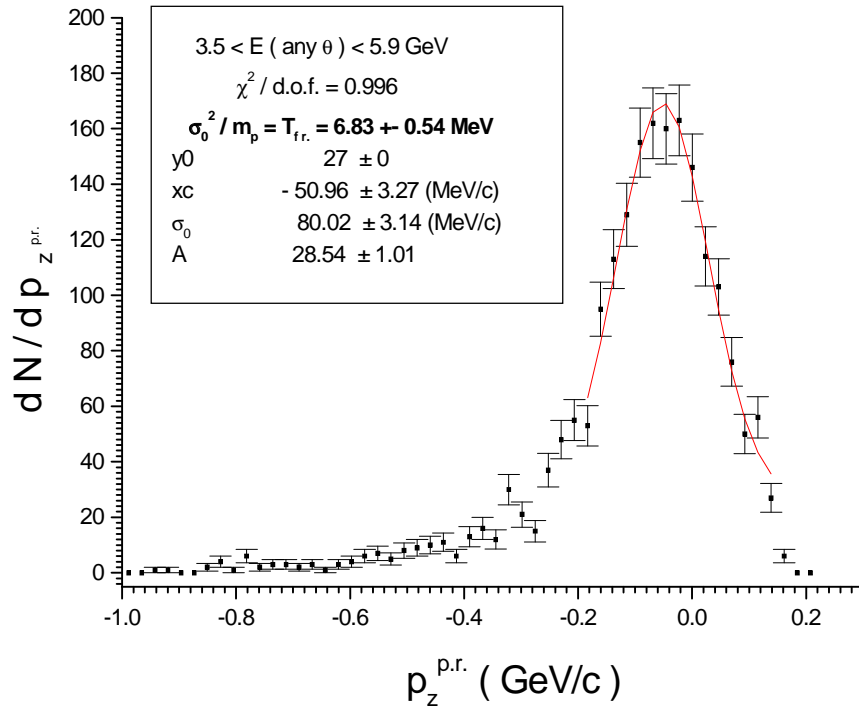


Fig. 10. – The experimental longitudinal momentum distribution of the protons in the fragmenting nucleus rest frame for ${}^4\text{He}+{}^7\text{Li}$ interactions at 4.5 A GeV/c incident momentum fitted with a Gaussian distribution.

We applied the same procedure on the projectile protons as obtained in nuclear ${}^4\text{He}+{}^7\text{Li}$ interactions simulated with **R**elativistic **Q**uantum **M**olecular **D**ynamics (RQMD 2.4). The first step was to determine which set of physical hypotheses fits best the experimental distribution (see e.g. Fig. 11).

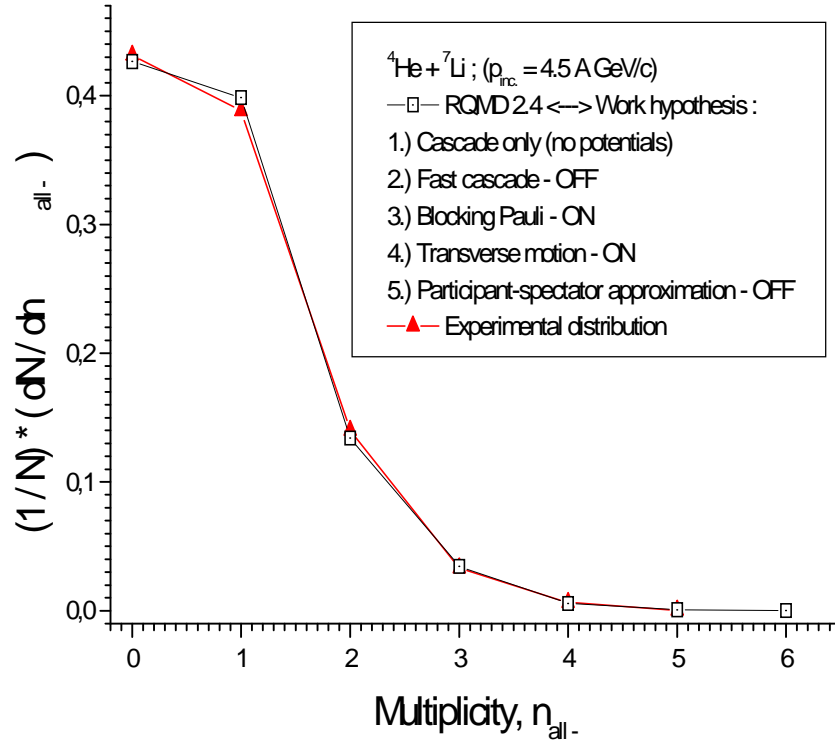


Fig. 11. – The experimental multiplicity distribution of the negative particles for ${}^4\text{He}+{}^7\text{Li}$ collisions at 4.6 A GeV incident energy compared with the analogous RQMD 2.4 distribution for five imposed hypotheses.

By using the physical hypotheses set found acceptable to the experimental output and by fitting the RQMD 2.4 kinetic energy distribution of the protons in the projectile rest frame with a Maxwell distribution one can find an apparent temperature value reasonably close to the experimental one $T = 6.75 \pm 0.18 \text{ MeV}$ ($\chi^2 / d.o.f. = 2.51$).

6. CONCLUSIONS

The results seem to point out a dependence of the projectile degree of excitation soon after nuclear collision occurred on the breakup topology. The width of the longitudinal momenta distribution as measured in the projectile rest frame was found to be closely linked to the projectile-target overlapping degree (Fig. 6). The estimator chosen for the presented analysis was the apparent temperature associated to a possible state of thermal equilibrium even though was used on a nuclear fragmenting system having small (${}^4\text{He}$) or relative small number of nucleons (${}^{40}\text{Ar}$).

The Goldhaber formula was thus improved by corroborating the projectile excitation hypothesis [15] with two corrections brought by Bertsch and Murphy [6,7], and by using the probability that identical nucleons having anticorrelated momenta to be close together in the coordinate space. We found apparent temperature values corresponding to a large variety of breakup channels by combining Eq.(2) with equation (35). Nevertheless, the applicability of the model described is limited. For heavy ion interactions, the model should provide radial flow calculations. The treatment of the projectile fragmentation sequential process requires also further investigation.

The apparent kinetic temperatures for the protons as projectile fragments were calculated by using two distinct methods. With the best set of physical hypotheses that fits best the experimental distributions for the RQMD 2.4 simulation program one can obtain temperature values in good agreement with the experimental ones. The results obtained suggested two possible nuclear fragmentation mechanisms: a sudden fragmentation by explosive mechanisms, shock wave-like type and a slow fragmentation by the “fission” of the spectator regions, mainly because of the interactions with the particles or fragments emitted from the participant region at transverse angles in CMS.

We continued the above studies by simulating the dynamics of an ensemble of A nucleons in a vibrating Woods-Saxon potential with couplings between collective and single-particle degrees of freedom. Initially, was imposed a wall frequency smaller than the single-particle one, corresponding to an oscillation period specific for low oscillating collective modes (adiabatic conditions). In the second place, the wall frequency was gradually increased close to the resonance frequency. One can expect for the last case that the divergence of the nucleon trajectories will reach a maximum. Thus, the fractal dimension of Poincare maps of the single-nucleon paths in phase-space (monopole case) varies from 0.8 to 1.23. Consequently, we may explain at low excitation energies the evaporation of nucleons and for higher energies it can be also implied a possible path towards nuclear fragmentation and multifragmentation as some of our future articles on this subject will show with much more rigors.

Acknowledgments. The authors wish to express their gratitude to SKM 200 Collaboration, especially to E. O. Okonov and G. L. Vardenga from the Joint Institute for Nuclear Research - Dubna (Russia). We are also indebted to H. Sorge for the RQMD 2.4 simulation program.

REFERENCES

1. H. H. HECKMAN *et al.*, *Proceedings of the 5th International Conference on High Energy Physics and Nuclear Structure*, Uppsala, Sweden, 1973, Elsevier, New York, 1974, p. 403.
2. H. FESHBACH, K. HUANG, *Phys. Letters*, **47B**, 300 (1973).
3. A. S. GOLDHABER, *Phys. Letters*, **53B**, 306 (1974).
4. J. V. LEPORE, J. RIDDELL, JR., *Proceedings, Lawrence Berkeley Lab. Lbl - 3675*, USA, 1974, p. 283.

5. D. E. GREINER, P. J. LINDSTROM, H. H. HECKMAN, B. CORK, F. S. BIESER, Phys. Rev. Lett., **35**, 152 (1975).
6. G. F. BERTSCH, Phys. Rev. Lett., **46**, 472 (1981).
7. M. J. MURPHY, Phys. Letters, **135B**, 25 (1984).
8. H. H. GAN, S. J. LEE, S. DAS GUPTA, J. BARRETTE, Phys. Letters, **B234**, 4 (1990).
9. F. P. BRADY *et al.*, Phys. Rev. Lett., **60**, 1699 (1988).
10. J. DREUTE, W. HEINRICH, G. RUSCH, B. WIEGEL, Phys. Rev. C, **44**, 1057 (1991).
11. H. H. HECKMAN, D. E. GREINER, P. J. LINDSTROM, F. S. BIESER, Phys. Rev. Lett., **28**, 926 (1972).
12. M. MUTHUSWAMY (E814 COLLABORATION), Nucl. Phys. A, **544**, 423c (1992).
13. A. SCHÜTTAUF *et al.*, Nucl. Phys. A, **607**, 457 (1996).
14. G. M. CHERNOV, K. G. GULAMOV, U. G. GULYAMOV, V. SH. NAVOTNY, N. V. PETROV, L. N. SVECHNIKOVA, B. JAKOBSSON, A. OSKARSSON, I. OTTERLUND, Nucl. Phys. A, **412**, 534 (1984).
15. W. BAUER, Phys. Rev. C, **51**, 803 (1995).
16. P. B. GOSSIAUX, R. PURI, CH. HARTNACK, J. AICHELIN, Nucl. Phys. A, **619**, 379 (1997).
17. A. S. BOTVINA *et al.*, Nucl. Phys. A, **584**, 737 (1995).
18. S. ALBERGO *et al.*, Nuovo Cimento, **89**, 1 (1985).
19. A. KOLOMIETS *et al.*, Phys. Rev. C, **54**, R472 (1996).
20. M. J. HUANG *et al.*, Phys. Rev. Lett., **78**, 1648 (1997).
21. F. GULMINELLI, D. DURAND, Nucl. Phys. A, **615**, 117 (1997).
22. J. P. BONDORF, A. S. BOTVINA, I. N. MISHUSTIN, Phys. Rev. C, **58**, 27 (1998).
23. V. SERFLING *et al.*, Phys. Rev. Lett., **80**, 3928 (1998).
24. D. J. MORRISSEY *et al.*, Annu. Rev. Nucl. Part. Science, **44**, 65 (1994).
25. J. POCHODZALLA *et al.*, Phys. Rev. C, **35**, 1695 (1987).
26. G. J. KUNDE *et al.*, Phys. Letters, **B272**, 202 (1991).
27. C. BESLIU, AL. JIPA, Rom. J. of Phys., **37**, 1011 (1992).
28. A. U. ABDURAKHIMOV *et al.*, Nucl. Phys. A, **362**, 376 (1981).
29. V. D. AKSINENKO *et al.*, Nucl. Phys. A, **348**, 518 (1980).
30. V. D. AKSINENKO *et al.*, Nucl. Phys. A, **324**, 266 (1979).
31. O. BENARY, R. PRICE, G. ALEXANDER, UCRL-20000 NN report, (1970).
32. R. HAGEDORN, *Relativistic Kinematics*, W. A. Benjamin, Inc., New York, 1963, p. 46.
33. P. R. BEVINGTON, D. K. ROBINSON, *Data Reduction and Error Analysis for the Physical Sciences*, McGraw-Hill, Inc., New York, 1992, p. 75.
34. O. SIMA, *Simularea Monte - Carlo a Transportului Radiațiilor*, Ed. ALL, Bucharest, 1994, p. 23.
35. E. J. MONIZ, I. SICK, R. R. WHITNEY, J. R. FICENEC, R. D. KEPHART, W. P. TROWER, Phys. Rev. Lett., **26**, 445 (1971).
36. L. D. LANDAU, E. M. LIFCHITZ, *Fizica Statistică*, 5th vol., 3rd edition, Ed. Tehnică, Bucharest, 1988, p. 160.
37. D. FELEA, C. BEȘLIU, V. TOPOR-POP, A. GHEAȚĂ, AL. JIPA, I.S. ZGURĂ, R. ZAHARIA, *Proceedings of the 8th International Conference on the Structure of Baryons - Baryons '98*, Bonn, Germany, 1998, Ed. World Scientific, Singapore, 1999, p. 705.
38. Y. P. VIYOGI, Phys. Rev. Lett., **42**, 33 (1979).
39. B. JAKOBSSON, R. KULLBERG, I. OTTERLUND, Lett. Nuovo Cimento, **15**, 444 (1976).
40. K.-H. SCHMIDT *et al.*, Nucl. Phys. A, **542**, 699 (1992).
41. E. HANELT *et al.*, Z. Phys. A, **346**, 43 (1993).
42. C. DONZAUD *et al.*, Nucl. Phys. A, **593**, 503 (1995).
43. J. REINHOLD, J. FRIESE, H.-J. KÖRNER, R. SCHNEIDER, K. ZEITELHACK, H. GEISSEL, A. MAGEL, G. MÜNZENBERG, K. SÜMMERER, Phys. Rev. C, **58**, 247 (1998).
44. J. FRIESE *et al.*, Nucl. Phys. A, **553**, 735c (1993).